PHYSICAL REVIEW B **85**, 245403 (2012)

Monitoring the formation of interface-confined mixture by photoelectron spectroscopy

Azzedine Bendounan,[1,*] Jürgen Braun,[2,†] Jan Minár,[2] Sven Bornemann,[2] Roman Fasel,[3] Oliver Gröning,[3] Yannick Fagot-Revurat,[4] Bertrand Kierren,[4] Daniel Malterre,[4] Fausto Sirotti,[1] and Hubert Ebert[2]

[1]*Synchrotron SOLEIL, L'Orme des Merisiers, Saint-Aubin, BP 48, F-91192 Gif-sur-Yvette Cedex, France*

[2]*Department Chemie, Ludwig-Maximilians Universität München, D-81377 München, Germany*

[3]*Empa, nanotech@surfaces Laboratory, Feuerwerkerstrasse 39, CH-3602 Thun, Switzerland*

[4]*Institut Jean Lamour, UMR 7198, Nancy-Université, BP 239, F-54506 Vandoeuvre-les-Nancy, France*

(Received 30 April 2012; published 4 June 2012)

We have investigated valence-band properties of Pt(111) surface covered by an Ag layer. Aside from showing significant changes in the *d* bands and the *sp*-like Shockley-type surface resonance depending on the thickness of the Ag layer, our spectroscopic data suggest the formation of an Ag-Pt mixture that progressively develops at the interface upon increasing the annealing temperature of the sample. On a 2-ML system, the Shockley resonance band is partially occupied and exhibits a large Rashba spin-orbit splitting that can be described by a first-principles band-structure calculation based on multiple-scattering theory. For the interface alloy, we have used the coherent potential approximation, which is one of the best models among the so-called single-site (local) theory. We observe a shift of the Shockley resonance due to the alloying process at the interface that probably favors the formation of the well-known triangular reconstruction.

DOI: 10.1103/PhysRevB.85.245403 PACS number(s): 73.20.At, 71.15.−m, 71.70.Ej, 79.60.−i

I. INTRODUCTION

Many physical properties such as those of transport and superconductivity rely strongly on the distribution of electrons close to the Fermi level (E_F).[1] For a given deposit/substrate system, this distribution is highly sensitive to the chemical composition at the surface and interface, the temperature, and the geometric structure. In particular, the formation of surface alloys, which is an important subject in material science, has a prominent role in surface chemical processes such as a heterogeneous catalysis.[2] It is also revealed to be promising for development of a new class of spintronic devices in the near future. The formation of ordered surface alloys upon adsorption of heavy metals on noble metal or on semiconductor surfaces greatly enhances the Rashba-type spin-orbit (RSO) coupling, due to hybridization between electronic valence states.[3–7] Similarly, the RSO splitting is modified when a nonordered alloy (i.e., random intermixing between the growing layer and the substrate) develops at the surface.[8,9] In general, two primary mechanisms can play a predominant role in the modification of electronic, chemical, and magnetic properties of ultrathin films covering conducting surfaces. First, due to the crystalline mismatch inducing an elastic strain, the average bond lengths between the atoms in the supported monolayer are typically different from those in the parent materials in their bulk states. Second, the strength of the bonding interaction, named the ligand effect, between the adsorbate atoms and the substrate can lead to significant changes in the surface electronic properties.[10,11] In the case of strong bonding and miscible elements, the surface can show the formation of an alloy, notably to release the elastic strain. Such effects are commonly analyzed by photoemission, either by probing core-level states or by measuring the evolution of the valence band, including the behavior of the surface state.[12] The latter is strongly sensitive to different types of adsorbates[13–16] and can even track the formation of, e.g., faulted stacking at the interface, which results in general from a relaxation of strains in the system through a creation of dislocation loops.[17] In this contest, we have recently found a partially occupied Shockley-type surface resonance on a Ag/Pt(111) system with a binding energy and a RSO splitting amplitude, both depending on the thickness of the Ag layer.[18] In continuation of this work, we present here a quantitative description of modifications in the Pt(111) valence band induced through segregation processes caused by deposition of an Ag layer followed by an annealing of the sample. The evolution of the surface resonance as a function of the annealing temperature has been investigated by angle-resolved photoemission spectroscopy (ARPES) and directly compared to theoretical one-step photoemission calculations. A pronounced effect on the energetics of the surface resonance due to temperature-induced segregation of Pt atoms at the Pt/Ag interface structure is clearly observed in our measurements. In detail, we discuss the migration of Pt atoms into the adjacent Ag-interface monolayer that occurs depending on the annealing temperature. In contrast to homogeneous surface potentials on pure metals, a random surface potential induced by segregated Pt atoms is expected to influence the electronic structure of the surface significantly. From the theoretical point of view, a relatively simple intermetallic binary alloy serves as an ideal candidate to challenge and demonstrate the capability of modern calculational concepts to perform quantitative photoemission analysis on disordered systems based on fully relativistic electronic-structure calculations for a semi-infinite half-space configuration. The challenge lies in the demand to successfully combine electronic-structure calculational techniques that allow treating in a fully relativistic mode the aspects of chemical disorder, segregation, and surface effects and to incorporate this in a one-step photoemission model. The paper is organized as follows: In Sec. II, we present the experimental details. In Sec. III, we briefly introduce the fully relativistic photoemission theory for disordered alloys and we discuss the corresponding computational details. Section IV is devoted to our experimental and theoretical results. A summary is given in Sec. V.

II. EXPERIMENTAL DETAILS

The valence-band spectra have been taken with a high-resolution photoelectron analyzer SES200 in combination with a VUV lamp (SPECS) for the photoexcitation. For the surface resonance band, and to improve the signal-to-background ratio, we have used a synchrotron radiation facility, which offers the possibility of changing the photon energy and light polarization. Hence, a part of the experiments has been performed at the X09LA-SIS beamline of the Swiss Light Source at Paul Scherrer Institut and was completed at TEMPO beamline of synchrotron SOLEIL. The entire ARPES spectra were collected at 50 K, and the appropriate orientation was fixed with the aid of low-energy electron diffraction (LEED). The Pt(111) substrate was cleaned by repeated cycles of Ar^+ ion sputtering, annealing under 1×10^{-8} mbar of oxygen at 800 K and then flashing at 1200 K in ultrahigh vacuum. This procedure was proven to lead to a clean surface with very high crystalline quality. The Ag films were deposited on a clean Pt(111) substrate kept at room temperature (RT) during evaporation. Then, successive annealings of the sample at different temperatures have been made according to the requirement of our experiment. The Ag deposition has been realized by using a Knudsen cell evaporator, and the flux has been calibrated by LEED and also after looking at the shape of the valence bands.

III. THEORETICAL AND COMPUTATIONAL DETAILS

A. Theoretical model

To achieve a reliable and detailed interpretation of the experimental spectra, it is inevitable to deal quantitatively with the wave vector and energy dependence of the transition-matrix elements. Also, a realistic description of the surface barrier is essential for a quantitative description of surface states and resonances of simple metals as well as of more complex structures such as thin films and multilayers. The most successful theoretical approach to deal with photoemission is the so-called one-step model as originally worked out in detail by Pendry and co-workers.[19] Therefore, we briefly discuss here the main features of the one-step model with a special emphasis on alloy systems.

The photocurrent in the so-called one-step model description is defined by Pendry's formula[19]

$$I^{\mathrm{PES}} \propto \mathrm{Im}\langle \epsilon_f, \mathbf{k}_\parallel | G_2^+ \Delta G_1^+ \Delta^\dagger G_2^- | \epsilon_f, \mathbf{k}_\parallel \rangle \, . \tag{1}$$

The expression can be derived from Fermi's golden rule for the transition probability per unit time[20] and therefore denotes the elastic part of the photocurrent. Inelastic energy losses and corresponding quantum mechanical interference terms[19–21] are excluded. Furthermore, the sudden approximation for the outgoing photoelectron is applied. The photoelectron state at the detector is written as $|\epsilon_f, \mathbf{k}_\parallel\rangle$, where $\mathbf{k}_\parallel$ denotes the component of the wave vector parallel to the surface, and ϵ_f is the kinetic energy of the photoelectron. In the fully relativistic formulation, $|\epsilon_f, \mathbf{k}_\parallel\rangle$ is understood as a four-component Dirac spinor. Via the advanced Green's matrix G_2^- in Eq. (1), all multiple-scattering events at ϵ_f are considered and the final state can be written as $|\Psi_f\rangle = G_2^- |\epsilon_f, \mathbf{k}_\parallel\rangle$. Using the standard layer Korringa-Kohn-Rostoker (KKR) method[22,23] generalized for the relativistic case,[24] the final state can be obtained as a time-reversed spin-polarized LEED (SPLEED) state. Lifetime effects are included phenomenologically in the SPLEED calculation by use of a parametrized, weakly energy-dependent, and complex inner potential $V_0(E_2) = V_{0\mathrm{r}}(E_2) + iV_{0\mathrm{i}}(E_2)$ as used conventionally.[20,25] The real part of $V_0(E_2)$ serves as a reference energy inside the solid with respect to the vacuum level.[26] The imaginary part $V_{0\mathrm{i}}(E_2)$ corresponds to an inelastic attenuation length of the scattered photoelectrons.

Following Durham,[27,28] we obtain the averaged photocurrent for an alloy as follows:[29]

$$\begin{aligned}\langle I^{\mathrm{PES}}(\epsilon_f, \mathbf{k}_\parallel)\rangle = {} & \langle I^{\mathrm{a}}(\epsilon_f, \mathbf{k}_\parallel)\rangle + \langle I^{\mathrm{m}}(\epsilon_f, \mathbf{k}_\parallel)\rangle \\ & + \langle I^{\mathrm{s}}(\epsilon_f, \mathbf{k}_\parallel)\rangle + \langle I^{\mathrm{inc}}(\epsilon_f, \mathbf{k}_\parallel)\rangle .\end{aligned} \tag{2}$$

For the atomic contribution, the averaging procedure is trivial since $\langle I^{\mathrm{a}}(\epsilon_f, \mathbf{k}_\parallel)\rangle$ is a single-site quantity. The atomic contribution is built up by a product between the matrix $\mathcal{Z}^{\mathrm{a}}_{jn\alpha_n}$ and the coherent multiple-scattering coefficients $A^c_{jn\Lambda}$ of the final state.[24] Herein, n denotes the nth cell of the jth layer and Λ denotes again the combined relativistic index (κ, μ). For the photocurrent, one gets this way

$$\langle I^{\mathrm{a}}(\epsilon_f, \mathbf{k}_\parallel)\rangle \propto \mathrm{Im} \sum_{\substack{jn\alpha_n \\ \Lambda\Lambda'}} c_{jn\alpha_n} A^c_{jn\Lambda} \mathcal{Z}^{\mathrm{a}}_{\substack{jn\alpha_n \\ \Lambda\Lambda'}} A^{c*}_{jn\Lambda'}, \tag{3}$$

where α_n denotes the different atomic species located at a given atomic site n of the jth layer. The corresponding concentration is given by $c_{jn\alpha_n}$.

For an explicit calculation, $\mathcal{Z}^{\mathrm{a}}$ must be separated into angular matrix elements and radial double matrix elements. A detailed description of the matrix $\mathcal{Z}^{\mathrm{a}}$ and of the multiple-scattering coefficients $A^c_{jn\Lambda}$ for the different atomic species is given in Ref. 24.

The intra(inter)layer contributions $\langle I^{\mathrm{m}}(\epsilon_f, \mathbf{k}_\parallel)\rangle$ to the photocurrent describe the multiple-scattering corrections of the initial state G_1^+ between and within the layers of the single crystal. They can be written in a similar form[29]

$$\langle I^{\mathrm{m}}(\epsilon_f, \mathbf{k}_\parallel)\rangle \propto \mathrm{Im} \sum_{\substack{jn \\ \Lambda\Lambda'}} A^c_{jn\Lambda} \, \mathcal{Z}^{c(2)}_{\substack{jn \\ \Lambda\Lambda'}} \, C^{B,G}_{jn\Lambda'} \, . \tag{4}$$

In analogy to the atomic contribution, the coherent matrix $\mathcal{Z}^{c(2)}$ can be separated into angular and radial parts. The difference to the atomic contribution is that the radial part of the matrix $\mathcal{Z}^{c(2)}$ consists of radial single matrix elements instead of radial double integrals. For details concerning the matrix elements and corresponding coefficients, the reader is referred to Ref. 29.

The contribution $\langle I^{\mathrm{s}}(\epsilon_f, \mathbf{k}_\parallel)\rangle$ accounts for the surface of the semi-infinite crystal. According to Durham,[27] the surface contribution remains unchanged compared to the ordered case: $\langle I^{\mathrm{s}}(\epsilon_f, \mathbf{k}_\parallel)\rangle = I^{\mathrm{s}}(\epsilon_f, \mathbf{k}_\parallel)$. The last contribution to the alloy photocurrent is the so-called incoherent part $\langle I^{\mathrm{inc}}(\epsilon_f, \mathbf{k}_\parallel)\rangle$

defined as

$$\langle I^{\rm inc}(\epsilon_f,\mathbf{k}_\parallel)\rangle \propto \sum_{\substack{jn\alpha_n \\ \Lambda\Lambda'\Lambda''}} c_{jn\alpha_n} A^c_{jn\Lambda} \mathcal{Z}^{(1)}_{\substack{jn\alpha_n \\ \Lambda\Lambda'}} \times \left(\tau^{00}_{jn\alpha_n} - t_{jn\alpha_n}\right)_{\Lambda'\Lambda''} \mathcal{Z}^{(2)}_{\substack{jn\alpha_n \\ \Lambda''\Lambda'''}} A^{c*}_{jn\Lambda'''} + \sum_{\substack{jn \\ \Lambda\Lambda'}} A^c_{jn\Lambda} \mathcal{Z}^{c(1)}_{\substack{jn \\ \Lambda\Lambda'}} \tau^{00}_{\substack{cjn \\ \Lambda'\Lambda''}} \mathcal{Z}^{c(2)}_{\substack{jn \\ \Lambda''\Lambda'''}} A^{c*}_{jn\Lambda'''}, \quad (5)$$

where $\tau^{00}_{jn\alpha_n}$ denotes the one-site restricted average coherent potential approximation (CPA) matrix for species α_n at atomic site n for layer j. τ^{00}_{cjn} represents the corresponding matrix for the coherent medium. The incoherent part $\langle I^{\rm inc}(\epsilon_f,\mathbf{k}_\parallel)\rangle$ completes the CPA-averaged photocurrent within the fully relativistic one-step model.

B. Computational details

The electronic structure is described within the framework of the fully relativistic Korringa-Kohn-Rostoker multiple-scattering theory[30] (SPRKKR) using the coherent potential approximation alloy theory. An appealing feature of the multiple-scattering formalism is the possibility to deal with substitutionally disordered materials within the CPA. The CPA is considered to be the best theory among the so-called single-site (local) alloy theories that assume complete random disorder and ignore short-range order. As Pt and Ag are immiscible in principle, the nonlocal version of the CPA (Ref. 31) should be used to account for short-range order, but the application of this method for the two-dimensional case is very tricky and extremely time consuming. In addition, one has to stress that the technical details of the combination of the nonlocal CPA and the one-step model of photoemission have not yet worked out. On the other hand, one would expect at least moderate changes in the bulk-electronic structure and only small changes concerning the energetic position of the sp-like surface state.

For the photoemission calculations, we used the new version of the fully relativistic one-step model,[29] which is an appropriate generalization of the original work on disordered alloys of Durham and Ginatempo.[27,28] Lifetime effects in the initial states have been included via a small constant imaginary value of $iV_{\rm i} = 0.05$ eV to represent scattering events by structural disorder and other incoherent processes. For the final states, a constant imaginary part $iV_{\rm f} = 2.0$ eV has been chosen again in a phenomenological way, independent on the concentration x. A realistic description of the surface potential is given through a spin-dependent Rundgren-Malmström barrier,[32] which connects the asymptotic regime $z < z_A$ to the bulk muffin-tin zero $V_{\rm or}$ by a third-order polynomial in z, spanning the range $z_A < z < z_E$. The values of the three parameters z_I, z_A, and z_E, which are in accordance with the experimental spectra, are the following: $z_I = -1.70$ a.u., $z_A = -3.2$ a.u., and $z_E = 0.0$ a.u..

IV. RESULTS AND DISCUSSION

Among the various possible transition-metal surface layer systems, Ag/Pt(111) is one of the most striking exceptions with a very limited solubility and a broad miscibility gap in the bulk.[33,34] It is characterized by a sharp interface at room temperature, as predicted from the phase diagram.[35] In the following, we present a description of its valence-band electronic structure. Figure 1 shows angle-integrated photoelectron spectra recorded near normal emission on clean and Ag-covered Pt(111) surfaces. It shows in particular the spectral changes in the valence band as a function of the Ag thickness and the annealing temperature. Concerning the Pt(111) spectrum, two main features associated with the 5d bands of Pt are seen in the energy range between 6 and 0.8 eV, followed by a continuum of sp states in the region close to E_F.[36] As soon as Ag is deposited, the shape of the Pt 5d bands changes and their intensity progressively diminishes with increasing the thickness of the Ag coverage. Simultaneously, new structures corresponding to the Ag 4d bands occur and dominate at higher coverage. In fact, in the photoemission spectra of clean Ag(111), electron emission from the Ag 4d levels appear between 3 and 7 eV and therefore overlap with the main features of the Pt 5d bands. However, based on studies on similar systems, e.g., Ag/Cu(111),[37] we expect the presence of a double-peak structure in the submonolayer regime which is associated to Ag $4d_{5/2}$ states that gradually grows up with the Ag-layer thickness (see Fig. 3 of Ref. 37). At elevated coverage [$\geqslant$1 monolayer (ML)], weak shoulders appear at $\sim$6 eV, which arise from the Ag $4d_{3/2}$ states and reflect the transition from atomic-to-solid state of Ag. The cross section

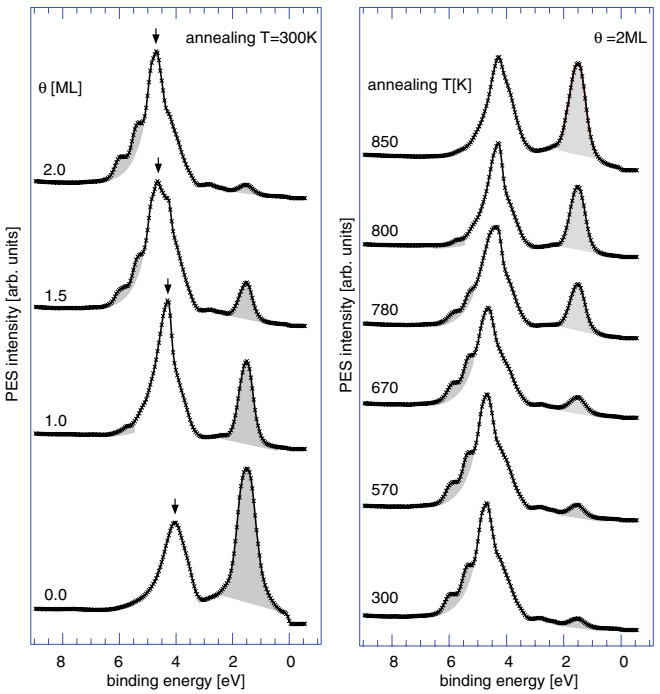

FIG. 1. (Color online) Valence-band spectra measured with HeI excitation energy on Pt(111) surface covered by Ag layers. The left panel shows the evolution of the d bands with the film thickness, and the right panel illustrates the changes in the valence band of 2-ML Ag/Pt(111) upon annealing of the sample.

of the Ag 4*d* states in photoemission is larger than that of Pt 5*d* states and, consequently, an apparent shift of the *d*-band center is observed as indicated by arrows in Fig. 1.

The evolution of the valence band of 2-ML Ag/Pt(111) as a function of the annealing temperature is shown in the right panel of Fig. 1. Only a slight modification is seen for an annealing up to 670 K. Above this temperature, one observes a steep increase in the Pt 5*d* signal at the expense of the Ag 4*d* bands. On the one hand, the intensity of the Pt feature at 1.8 eV continuously increases, and on the other hand, the shoulders associated with pure 2-ML islands are progressively weaken. We believe that these spectroscopical changes in the *d* bands are due to the formation of a two-dimensional alloy, as it has been demonstrated in the case of the submonolayer regime, where the surface exhibits a pseudormophic structure at room temperature[38,39] and develops into an alloy upon annealing to temperatures above 620 K.[40–43] Depending on the Ag coverage, a formation of either a droplet or stripe domain patterns has been observed.[40–43] A similar behavior was also seen when the Ag submonolayer is deposited on Pt(100) substrate.[44,45] However, previous investigations on an annealed 2-ML Ag/Pt(111) system have shown that the surface top monolayer consists of Ag atoms only.[46,47] This means that, in this case, the alloy is strictly confined at the interface. It can consist of Ag atoms or nanoclusters dissolved in the uppermost plane of the Pt substrate and of Pt atoms or nanoclusters segregated in the neighbor Ag monolayer.

For the annealing temperature T $\sim$ 800 K, the resulting spectrum resembles the one measured for 1 ML prepared at RT. As proved by temperature programed desorption studies,[48] the annealing at a high temperature provokes a desorption of the second top ML, while the first ML stays sticking to the substrate.

In this part, we examine the sensitivity of the surface resonance to the annealing of the sample. First, to remind briefly, the Pt(111) surface has an empty Shockley state around the center $\bar{\Gamma}$ of the surface Brillouin zone (SBZ) with a larger RSO splitting[18] when compared to Au(111).[49,50] Deposition of 2-ML Ag on Pt(111) induces a shift down in energy for the Shockley state and leads to an increased RSO splitting as well as to a variation of the effective mass (Fig. 2). For higher Ag coverages, a reversed shift of the surface resonance to lower binding energies is observed.[18] Supported by the experimental results, our theoretical analysis shows that the influence of the spin-orbit coupling is transferred via multiple scatterings between the semi-infinite bulk and the surface potential. Also, a pronounced variation of the effective mass as a function of the Ag film thickness has been observed.[18] As illustrated in Fig. 2, a straight *X*-shaped structure is seen in the ARPES data. One can observe a clear difference in the band curvature between the experiment and the theory, which suggests a significant modification of the in-plane surface potential. In fact, the present system exhibits a variety of surface reconstructions depending on the coverage of the Ag layer and the annealing temperature. For example, on 2 ML, the stripes or the domain walls characterizing the surface have been identified as regions with low electron density.[51] Moreover, a significant variation of the local work function has been measured between the fcc and hcp stackings.[52] Our simulations do not take into the account the surface structure effect. This is partly the origin of

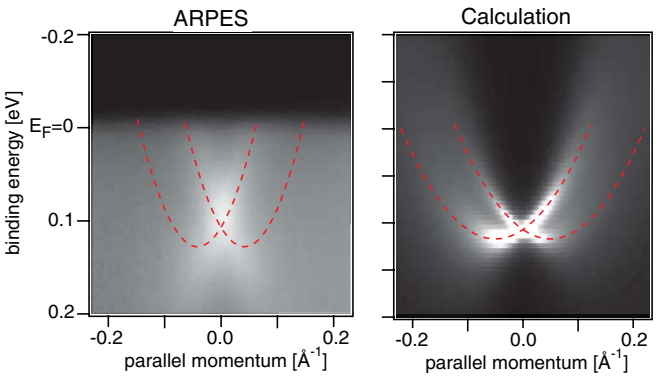

FIG. 2. (Color online) Surface resonance bands obtained by ARPES measurements (left panel) and by first-principles calculations (right panel) for 2 ML of Ag on Pt(111) surface. The ARPES data have been recorded at normal emission along the $\bar{\Gamma}$-$\bar{K}$ direction and at $T = 50$ K with a photon energy h$\nu = 20$ eV. The photoemission calculations include a surface potential correction (more detail see text).

the observed discrepancy in the effective mass. In addition, a systematic error is introduced when using the local spin density approximation (LSDA) that affects significantly the complete energetic of the Shockley surface resonance. In other words, the shape of the barrier potential near the surface and connected with this the theoretical description of the charge distribution within the first few vacuum layers are only semiquantitatively correct when the LSDA approach is used and can not be compensated by the use of a model barrier with the correct long-range behavior. The same argument should be applied to other bulk-induced surface states or surface resonances because of the general shortcomings of the LSDA.

Figure 3 presents the normal emission spectra measured by ARPES on a 2-ML film deposited on Pt(111), before and after annealing, together with the calculated spectrum for Pt(111). On the film deposited at RT, the surface resonance is found at a binding energy of $\sim$0.107 eV. It is associated with a surface characterized by ordered metastable superstructure patterns consisting of alternating domains with fcc and hcp stacking separated by partial misfit dislocation lines seen as dark stripes in the STM images,[53] as in the case of the Au(111) surface. The stripes represent domain walls in which the strain is relieved and are characterized by locally low electron density.[51] The periodicity of this reconstruction has been estimated to correspond to a $(\sqrt{3} \times p)$ unit cell with $p = (14 \pm 1)$.[53]

Even after a slight annealing at 600 K, a clear change of the surface resonance energy is observed (Fig. 3). It shifts continuously upon increasing the annealing temperature. According to the *d*-band spectra, the shift is attributed to a structural modification of the system that induces a modification of the surface potential. As discussed above, we have demonstrated that the annealing of the sample leads to a migration of Pt atoms into the Ag interface monolayer and to an incorporation of Ag atoms into the uppermost plane of the Pt(111) substrate. In addition, we observe an increase in the peak linewidth with the annealing temperature, which reflects the presence of defects produced by the alloy formation. Indeed, we believe that the Ag-Pt mixture at the interface underneath the Ag

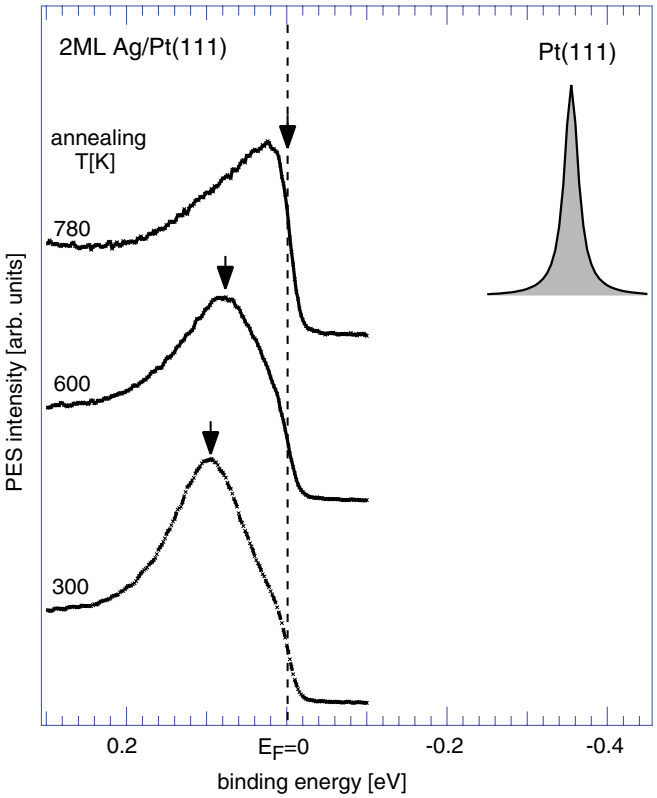

FIG. 3. (Color online) Normal emission spectra measured at 50 K on 2 ML of Ag/Pt(111) annealed at different temperatures, together with the spectrum of bare Pt(111) (shaded area) obtained by first-principles band-structure calculations that would show up in an inverse photoemission experiment.

topmost monolayer causes a pronounced roughness of the surface. At annealing temperature T $\sim$ 780 K, the surface resonance is exactly positioned at E_F. At this temperature, a formation of a triangularlike surface superstructure is observed with a periodicity estimated to be close to a (24×24) Ag unit cell.[46] The superstructure was described as due to partial dislocations in the Ag layer.[46,53] Here, our investigations on 2-ML Ag/Pt(111) suggest that the strong misfit stress in the system, which is due to both the lattice mismatch ($\sim$4.3%) and the charge transfer from Ag to Pt, is released by the creation of an Ag-Pt intermixing strictly confined at the interface and partial misfit dislocations that develop in the upper planes of the Pt(111) substrate. In other words, one can expect a two-phase coexistence of an Ag-Pt alloying phase in the interface region and a misfit dislocations phase from underneath. The misfit dislocations give rise to the depletion regions observed in the STM images[46,54] as dark lines surrounding triangle patterns where the stacking faults are located. The phenomenon of the two-phase coexistence has also been observed for Ag submonolayer on Pt(100) and was discussed in terms of two competing mechanisms. The competition results in a reduced surface stress.[44] Both processes, alloying and dislocation, affect significantly the surface electronic structure and induce modifications of binding energies, effective masses, peak linewidths, and RSO splittings, as revealed for other systems.[3,8,9,17]

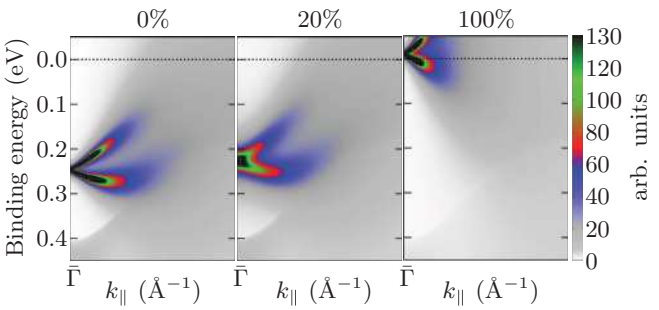

FIG. 4. (Color online) Spectral functions for semi-infinite half-space configurations obtained by first-principles calculations on 2-ML Ag/Pt(111) system with different compositions at the interface. From left to right: 100% Ag in the first deposited Ag ML, 80% Ag with 20% Pt in the first deposited Ag ML, and fully 100% Pt replacing Ag in the first ML [corresponding to the 1-ML Ag/Pt(111) system].

On the other hand, the fact that the surface resonance develops exactly at E_F can help to explore further physical properties based on electronic excitations such as many-body effects.[55] Moreover, this surface showing long-range triangular patterns has served as a template for self-organization process of metallic and organic nanostructures.[46,56] Then, one can expect that the high electron population at E_F plays an essential role in this process. At T $\geqslant$ 800 K, the ARPES spectrum shows no features near E_F, implying that the surface resonance becomes unoccupied and is presumably located close to the energetic position corresponding to the 1-ML system. This is in good agreement with the d-band behavior (shown in Fig. 1), suggesting a desorption of the second topmost Ag monolayer.

In Fig. 4, we report band-structure calculations performed with different concentrations of Pt atoms segregated into the first Ag monolayer, while the topmost Ag monolayer contains 100% Ag in all cases. The details of the calculational procedure are given elsewhere.[18] Shown are spectral functions obtained self-consistently for semi-infinite half-space configurations with corresponding Pt concentrations in the first Ag monolayer. For 100% Ag concentration in the first monolayer, the surface resonance appears at a binding energy of about 0.25 eV. It shifts progressively to lower binding energies upon increasing the Pt concentration and appears at a minimum binding energy for 100% concentration of Pt atoms replacing Ag in the first monolayer (bearing in mind that the top monolayer is 100% Ag), which corresponds to the case of 1-ML Ag/Pt(111) system. Although the experimental trend is reproduced in a qualitative sense, a closer inspection of the energetic position reveals that no full quantitative agreement has been achieved between experiment and theory. The reason is found in the insufficient description of the vacuum half-space when using the local density approximation. This point has been discussed in detail, for example, in Ref. 18. From the bare spectral function calculations, we found for all concentrations of Pt atoms in the first Ag monolayer a systematic overestimation of the binding energy of about 0.14 eV. This is clearly observable from Fig. 4 when moving from left to right. To obtain quantitative agreement with the experimental binding energies as a function of the Pt concentration, we had to use a model barrier with the correct long-range behavior. In

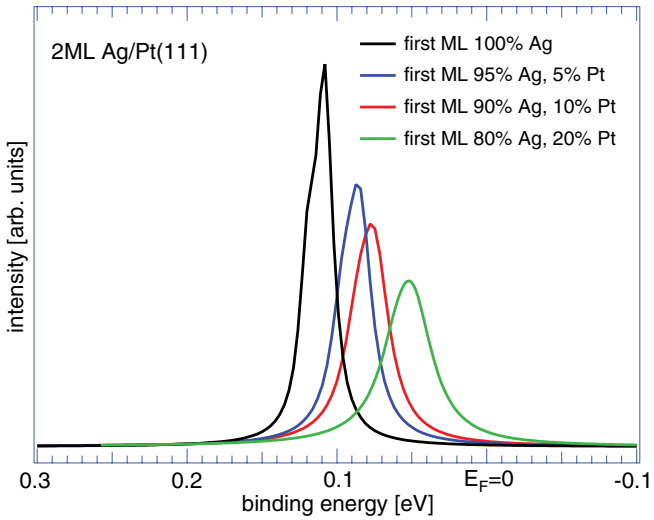

FIG. 5. (Color online) Normal emission spectra obtained by first-principles calculations on 2-ML Ag/Pt(111) system with different compositions at the interface: (dark) 100% Ag in the first deposited Ag ML; (blue) 95% Ag and 5% Pt in the first deposited Ag ML; (red) 90% Ag with 10% Pt in the first deposited Ag ML; and (green) 80% Ag with 20% Pt in the first deposited Ag ML.

our case, the corresponding spectroscopical calculations are based on a Rundgren-Malmström–type surface barrier.[18] For all three surface-alloy systems, we fixed the barrier parameters for the image-plane values and for the polynomial region exactly to the values we used for the previous layer-dependent photoemission study on the pure double-layer system.[18] In addition, we used for all three alloy systems the same work function value. Its value (4.75 eV) is identical to that of the pure double-layer system because we do not expect a change in this value due to a small amount of Pt atoms segregated in the first Ag monolayer. The spectroscopical data for normal emission at 20 eV photon energy are presented in Fig. 5.

Compared to the bare spectral function calculations, we observe a progressive shift of the surface resonance towards E_F, which reflects more or less perfectly the experimental results. This shift in the binding energy is due to the heuristic correction of the surface electronic structure defined in terms of the model barrier. For the pure 2-ML system, we found from our former investigation a binding energy of 107 meV in quantitative agreement to the experiment.[18] Here, the surface resonance moves from about 107 to 86 meV for 5%, to 77 meV for 10%, and to 52 meV for 20% Pt, keeping all barrier parameters fixed. We also found from the calculations that the SO splitting appears only slightly affected by the structural change in the system, which is presumably due to the fact that the mixing is only confined to the interface.

V. CONCLUSIONS

In summary, we have presented a detailed photoemission study on the modifications of the *d* band and the Rashba-split surface resonance of a 2-ML Ag/Pt(111) system as a function of the annealing temperature of the sample. The results, which are supported by first-principles calculations, suggest the existence of a thermally activated intermixing process confined at the Ag-Pt interface, which consists of a migration of Ag atoms into the Pt(111) surface and a segregation of the Pt atoms into the Ag first monolayer, and consequently leads to the formation of an alloy. This process, together with the presence of partial misfit dislocations in the upper planes of the Pt(111) substrate, allows the interface to be relieved of the misfit stress. The existence of the two mechanisms probably favors the formation of the well-known triangular reconstruction on the surface of the 2-ML system. This finding appears in good agreement with the results of recent investigations showing that the dislocations are buried into the Pt(111) substrate.[54,57] On the other hand, the calculational results show again the strong need on a quantitative description of the vacuum half-space within a self-consistent electronic-structure method which respects the correct long-range behavior of the surface potential.

ACKNOWLEDGMENTS

We gratefully acknowledge the beamline staff of X09LA at the Swiss Light Source for their excellent technical support. Also, many thanks to TEMPO beamline staff, in particular Ch. Chauvet, for their assistance. We kindly thank V. Esaulov for his careful reading of the manuscript. Financial support from the Deutsche Forschungsgemeinschaft (Grant No. EBE-154/18) and the Bundesminsisterium für Bildung und Forschung (Grants No. 05KIOWW1/2, No. 05KSI-WMB/1, and No. 05 SC8BDA 2) is gratefully acknowledged.

*azzedine.bendounan@synchrotron-soleil.fr
†juergen.braun@cup.uni-muenchen.de

[1] Y. Guo, Y. F. Zhang, X. Y. Bao, T. Z. Han, Z. Tang, L. X. Zhang, W. G. Zhu, E. G. Wang, Q. Niu, Z. Q. Qiu, J. F. Jia, Z. X. Zhao, and Q. K. Xue, Science **306**, 1915 (2004).

[2] F. Besenbacher, I. Chorkendorff, B. S. Clausen, B. Hammer, A. M. Molenbroek, J. K. Norskov, and I. Stensgaard, Science **279**, 1913 (1998).

[3] C. R. Ast, J. Henk, A. Ernst, L. Moreschini, M. C. Falub, D. Pacilé, P. Bruno, K. Kern, and M. Grioni, Phys. Rev. Lett. **98**, 186807 (2007).

[4] J. Nitta, T. Akazaki, H. Takayanagi, and T. Enoki, Phys. Rev. Lett. **78**, 1335 (1997).

[5] K. Sakamoto, H. Kakuta, K. Sugawara, K. Miyamoto, A. Kimura, T. Kuzumaki, N. Ueno, E. Annese, J. Fujii, A. Kodama, T. Shishidou, H. Namatame, M. Taniguchi, T. Sato, T. Takahashi, and T. Oguchi, Phys. Rev. Lett. **103**, 156801 (2009).

[6] L. Moreschini, A. Bendounan, I. Gierz, C. R. Ast, H. Mirhosseini, H. Höchst, K. Kern, J. Henk, A. Ernst, S. Ostanin, F. Reinert, and M. Grioni, Phys. Rev. B **79**, 075424 (2009).

[7] L. Moreschini, A. Bendounan, H. Bentmann, M. Assig, K. Kern, F. Reinert, J. Henk, C. R. Ast, and M. Grioni, Phys. Rev. B **80**, 035438 (2009).

[8] H. Cercellier, C. Didiot, Y. Fagot-Revurat, B. Kierren, L. Moreau, D. Malterre, and F. Reinert, Phys. Rev. B **73**, 195413 (2006).

[9]D. Malterre, B. Kierren, Y. Fagot-Revurat, S. Pons, A. Tejeda, C. Didiot, H. Cercellier, and A. Bendounan, New J. Phys. **9**, 391 (2007).
[10]J. R. Kitchin, J. K. Norskov, M. A. Barteau, and J. G. Chen, Phys. Rev. Lett. **93**, 156801 (2004).
[11]J. R. Kitchin, J. K. Norskov, M. A. Barteau, and J. G. Chen, J. Chem. Phys. **120**, 10240 (2004).
[12]S. Hüfner, *Photoelectron Spectroscopy Principles and Applications*, 3rd ed. (Springer, Berlin, 1995).
[13]F. Forster, A. Bendounan, J. Ziroff, and F. Reinert, Surf. Sci. **600**, 3870 (2006).
[14]F. Forster, A. Bendounan, F. Reinert, V. G. Grigoryan, and M. Springborg, Surf. Sci. **601**, 5595 (2007).
[15]J. Ziroff, P. Gold, A. Bendounan, F. Forster, and F. Reinert, Surf. Sci. **603**, 354 (2009).
[16]A. Scheybal, K. Müller, R. Bertschinger, M. Wahl, A. Bendounan, P. Aebi, and T. A. Jung, Phys. Rev. B **79**, 115406 (2009).
[17]A. Bendounan, H. Cercellier, B. Kierren, Y. Fagot-Revurat, V. Yu Yurov, and D. Malterre, Europhys. Lett. **64**, 392 (2003).
[18]A. Bendounan, K. Aït-Mansour, J. Braun, J. Minar, S. Bornemann, R. Fasel, O. Gröning, F. Sirotti, and H. Ebert, Phys. Rev. B **83**, 195427 (2011).
[19]J. B. Pendry, Surf. Sci. **57**, 679 (1976).
[20]G. Borstel, Appl. Phys. A **38**, 193 (1985).
[21]C. Caroli, D. Lederer-Rozenblatt, B. Roulet, and D. Saint-James, Phys. Rev. B**8**, 4552 (1973).
[22]J. Korringa, Physica (Amsterdam) **6/7**, 392 (1947).
[23]W. Kohn and N. Rostocker, Phys. Rev. **94**, 1111 (1954).
[24]J. Braun, Rep. Prog. Phys. **59**, 1267 (1996).
[25]J. B. Pendry, *Energy Electron Diffraction* (Academic, London, 1974).
[26]G. Hilgers, M. Potthoff, N. Müller, U. Heinzmann, L. Haunert, J. Braun, and G. Borstel, Phys. Rev. B **52**, 14859 (1995).
[27]P. J. Durham, J. Phys. F: Met. Phys. **11**, 2475 (1981).
[28]B. Ginatempo, P. J. Durham, and B. I. Gyorffy, J. Phys.: Condens. Matter **1**, 6483 (1989).
[29]J. Braun, J. Minár, F. Matthes, C. M. Schneider, and H. Ebert, Phys. Rev. B **82**, 024411 (2010).
[30]H. Ebert, D. Ködderitzsch, and J. Minár, Rep. Prog. Phys. **74**, 096501 (2011).
[31]P. R. Tulip, J. B. Staunton, S. Lowitzer, D. Ködderitzsch, and H. Ebert, Phys. Rev. B **77**, 165116 (2008).
[32]G. Malmström and J. Rundgren, Comput. Phys. Commun. **19**, 263 (1980).
[33]T. B. Massalski, *Binary Alloys Phase Diagram*, 2nd ed. (ASM International, Ohio, 1990), Vol. 3, p. 2998.
[34]H. Ebert, J. Abart, and J. Voitländer, J. Less-Common Met. **91**, 89 (1983).
[35]P. Durussel and P. Feschotte, J. Alloys Compd. **239**, 226 (1996).
[36]N. Memmel and E. Bertel, Phys. Rev. Lett. **75**, 485 (1995).
[37]B. Kierren, A. Bendounan, H. Cercellier, Y. Fagot-Revurat, F. Bertran, V. Yu Yurov, and D. Malterre, Phys. Low-Dim. Struct. **11/12**, 167 (2001).
[38]J. S. Tsay, Y. D. Yao, and C. S. Shern, Phys. Rev. B **58**, 3609 (1998).
[39]J. S. Tsay and C. S. Shern, J. Vac. Sci. Technol. **14**, 2522 (1996).
[40]P. Zeppenfeld, M. Krzyzowski, C. Romainczyk, G. Comsa, and M. G. Lagally, Phys. Rev. Lett. **72**, 2737 (1994).
[41]H. Röder, R. Schuster, H. Brune, and K. Kern, Phys. Rev. Lett. **71**, 2086 (1993).
[42]U. Strüber and J. Küppers, Surf. Sci. **294**, L924 (1993).
[43]P. Zeppenfeld, M. A. Krzyzowski, C. Romainczyk, R. David, G. Comsa, H. Röder, K. Bromann, H. Brune, and K. Kern, Surf. Sci. **342**, L1131 (1995).
[44]M. Batzill and B. E. Koel, Europhys. Lett. **64**, 70 (2003).
[45]M. Batzill and B. E. Koel, Surf. Sci. **553**, 50 (2004).
[46]H. Brune, M. Giovannini, K. Bromann, and K. Kern, Nature (London) **394**, 451 (1998).
[47]K. Aït-Mansour, P. Ruffieux, W. Xiao, P. Gröning, R. Fasel, and O. Gröning, Phys. Rev. B **74**, 195418 (2006).
[48]T. Härtel, U. Strüber, and J. Küppers, Thin Solid Films **229**, 163 (1993).
[49]J. Wiebe, F. Meier, K. Hashimoto, G. Bihlmayer, S. Blügel, P. Ferriani, S. Heinze, and R. Wiesendanger, Phys. Rev. B **72**, 193406 (2005).
[50]F. Reinert, J. Phys.: Condens. Matter. **15**, S693 (2003).
[51]H. Röder, K. Bromann, H. Brune, and K. Kern, Surf. Sci **376**, 13 (1997).
[52]P. Ruffieux, K. Aït-Mansour, A. Bendounan, R. Fasel, L. Patthey, P. Gröning, and O. Gröning, Phys. Rev. Lett. **102**, 086807 (2009).
[53]H. Brune, H. Röder, C. Boragno, and K. Kern, Phys. Rev. B **49**, 2997 (1994).
[54]K. Aït-Mansour, A. Buchsbaum, P. Ruffieux, M. Schmid, P. Gröning, P. Varga, R. Fasel, and O. Gröning, Nano Lett. **8**, 2035 (2008).
[55]P. M. Echenique, R. Berndt, E. V. Chulkov, T. Fauster, A. Goldmann, and U. Höfer, Surf. Sci. Rep. **52**, 219 (2004).
[56]K. Aït-Mansour, M. Treier, P. Ruffieux, M. Bieri, R. Jaafar, P. Gröning, R. Fasel, and O. Gröning, J. Phys. Chem. C **113**, 8407 (2009).
[57]K. Aït-Mansour, H. Brune, D. Passerone, M. Schmid, W. Xiao, P. Ruffieux, A. Buchsbaum, P. Varga, R. Fasel, and O. Gröning (unpublished).